journal of the mechanical behavior of biomedical materials 124 (2021) 104795

Contents lists available at ScienceDirect

Journal of the Mechanical Behavior of Biomedical Materials

journal homepage: www.elsevier.com/locate/jmbbm

Guide to mechanical characterization of articular cartilage and hydrogel constructs based on a systematic *in silico* parameter sensitivity analysis

Seyed Ali Elahi [a,b,*], Petri Tanska [c], Satanik Mukherjee [d,e], Rami K. Korhonen [c], Liesbet Geris [d,e,f], Ilse Jonkers [a], Nele Famaey [b]

[a] Human Movement Biomechanics Research Group, Department of Movement Sciences, KU Leuven, Leuven, Belgium
[b] Soft Tissue Biomechanics Group, Biomechanics Division, Mechanical Engineering Department, KU Leuven, Leuven, Belgium
[c] Department of Applied Physics, University of Eastern Finland, Kuopio, Finland
[d] Prometheus, Division of Skeletal Tissue Engineering, KU Leuven, Leuven, Belgium
[e] Biomechanics Section, KU Leuven, Leuven, Belgium
[f] GIGA in Silico Medicine, University of Liège, Liège, Belgium

ARTICLE INFO

Keywords:
Articular cartilage
Hydrogel construct
Tissue engineering
Inverse mechanical characterization
Parameter sensitivity analysis

ABSTRACT

Osteoarthritis is a whole joint disease with cartilage degeneration being an important manifestation. Tissue engineering treatment is a solution for repairing cartilage defects by implantation of chondrocyte-laden hydrogel constructs within the defect. *In silico* models have recently been introduced to simulate and optimize the design of these constructs. These models require accurate knowledge on the mechanical properties of the hydrogel constructs and cartilage explants, which are challenging to obtain due to their anisotropic structure and time-dependent behaviour.

We performed a systematic *in silico* parameter sensitivity analysis to find the most efficient unconfined compression testing protocols for mechanical characterization of hydrogel constructs and cartilage explants, with a minimum number of tests but maximum identifiability of the material parameters. The construct and explant were thereby modelled as porohyperelastic and fibril-reinforced poroelastic materials, respectively. Three commonly used loading regimes were simulated in Abaqus (ramp, relaxation and dynamic loading) with varying compressive strain magnitudes and rates. From these virtual experiments, the resulting material parameters were obtained for each combination using a numerical inverse identification scheme.

For hydrogels, maximum sensitivity to the different material parameters was found when using a single step ramp loading (20% compression with 10%/s rate) followed by 15 min relaxation. For cartilage explants, a two-stepped ramp loading (10% compression with 10%/s rate and 10% compression with 1%/s rate), each step followed by 15 min relaxation, yielded the maximum sensitivity to the different material parameters. With these protocols, the material parameters could be retrieved with the lowest amount of uncertainty (hydrogel: $< 2\%$ and cartilage: $< 6\%$). These specific results and the overall methodology can be used to optimize mechanical testing protocols to yield reliable material parameters for *in silico* models of cartilage and hydrogel constructs.

1. Introduction

The main function of articular cartilage is to provide near frictionless rotation of joints while absorbing shocks and minimizing peak loads in the underlying subchondral bone. Knee articular cartilage defects affect the mechanical integrity of the tissue, with malalignment or joint instability changing cartilage loading, potentially contributing to cartilage degeneration and the development of osteoarthritis (OA) (Beynnon et al., 2002; Li et al., 2020; NovarettiJoão et al., 2020; Shefelbine et al., 2006). Since cartilage does not contain any blood vessels (avascular) or nerves (aneural), it has a very limited self-healing capacity once damaged.

Tissue engineering (TE) treatments are a potential answer to OA joint repair. These rely on cell-based procedures (Brittberg et al., 1994; Jacobi et al., 2011) aiming to restore cartilage integrity. Hydrogel-based TE procedures aim at repairing large cartilage defects by implanting biological implants, *i.e.* chondrocyte-laden hydrogel constructs or scaffolds within the defects (Kundu et al., 2015). The chondrocyte is the only cell

* Corresponding author. Human Movement Biomechanics Research Group, Tervuursevest 101, box 1501, 3001, Leuven, Belgium.
E-mail address: seyedali.elahi@kuleuven.be (S.A. Elahi).

https://doi.org/10.1016/j.jmbbm.2021.104795
Received 4 June 2021; Received in revised form 7 August 2021; Accepted 21 August 2021
Available online 24 August 2021

type within the cartilage and is responsible for synthesizing extracellular matrix (ECM). The solid part of ECM is primarily composed of proteoglycans (PGs) and collagen fibrils (Mohammadi et al., 2013). Mechanical loading is crucial in stimulating ECM formation by chondrocytes (Kisiday et al., 2004).

Hydrogel constructs are often suggested as 'easy to use' scaffolds to embed chondrocytes for *in vivo* application. In this context, different hydrogel-based scaffolds have been proposed to enhance cartilage repair (Drury and Mooney, 2003). Alternatively, hydrogels are also being used to study mechano-transduction and -responsiveness of chondrocytes *in vitro*. Hydrogels are interesting scaffolds as they have a structure comparable to the extracellular matrix of cartilage (Hosseini et al., 2021). Although there are many appropriate materials for scaffolds, alginate has received much interest since it has lots of advantages for cartilage repair, including tunable mechanical characteristics and a simple production procedure (Farokhi et al., 2020). However, accurate mechanical characteristics and role of mechanical loading in cell-seeded alginates yet must be determined.

In the last decades, *in silico* modelling, or more specifically, finite element (FE) modelling has been used extensively to unravel the role of mechanical loading in cartilage degeneration and regeneration within the cell-seeded hydrogel implants for cartilage repair approaches (Wilson et al., 2005a; Mononen et al., 2016, 2018; Orozco et al., 2018; Kelly and Prendergast, 2006; Bandeiras and Completo, 2017; Zahedmanesh et al., 2014; Walter et al., 2019; Elahi et al., 2020). The mechanical properties of the cartilage and hydrogel implants are crucial parameters of these models. Thus, accurate mechanical characterization of the cartilage tissue and hydrogel is essential.

Measuring mechanical properties of soft tissues and particularly cartilage is highly challenging due to their anisotropic and heterogeneous structure (Elahi, 2018; Elahi et al., 2018). Mechanical characteristics of such tissues are typically approximated through inverse mechanical characterization methods, where constitutive and geometric models are developed of which the model parameters are then altered to achieve best match with corresponding experimental results (Evans, 2017).

Constitutive models of cartilage mechanics have been previously proposed by various groups (Li et al., 1999; DiSilvestro et al., 2001; Ateshian et al., 2009; Jones et al., 2016; Kazemi et al., 2013; Kazemi and Li, 2014; Ebrahimi et al., 2019; Babalola and Bonassar, 2009). Among these models, the fibril-reinforced poroelastic (FRPE) material model (Ebrahimi et al., 2019) has been shown to accurately predict the contribution of different constituents of cartilage tissue to its overall mechanical behaviour. As for hydrogel constructs, poroelastic (Babalola and Bonassar, 2009), poroviscoelastic (Nguyen et al., 2009a) and porohyperelastic material models have been used, among which the porohyperelastic material model most accurately simulates the behaviour of hydrogel constructs under mechanical loading (Zahedmanesh et al., 2014). It remains however a challenge to experimentally determine the different parameters that accurately describe their mechanical behaviour.

A variety of mechanical testing protocols have been reported in literature for cartilage and hydrogel constructs mechanical characterization (Ebrahimi et al., 2019; Nguyen et al., 2009a; Danso et al., 2018; Olvera et al., 2015; DiSilvestro and Suh, 2001; Wilson et al., 2005b; Ateshian et al., 2003; Patel et al., 2019). The prevalent testing configurations reported in literature are unconfined compression, confined compression and indentation. These testing configurations can be either load- or displacement-controlled, whereby the imposed variable follows a certain protocol which is typically a combination of ramps, relaxation phases and dynamic loading regimes at different magnitudes and rates. It is challenging to select the optimal testing protocol, *i.e.* one that probes the tissue in the relevant loading regime as well as allows to observe the effects of the different tissue constituents and hence material parameters.

Recently, based on a systematic literature review, Patel et al. (2019) provided a guide to the mechanical characterization of cartilage and hydrogel constructs. Yet, where this guide does an excellent job in trying to homogenize testing approaches between research groups, it does not consider if the suggested protocols are suited for reliably obtaining material parameters for subsequent *in silico* modeling. To this end, the sensitivity of the different testing protocols to the resulting material parameters, which depicts the identifiability of the material parameters using each testing protocol, has to be determined. The loading protocol that yields the highest sensitivity to the material parameters can be considered as the ideal protocol for material parameter characterization. Such a systematic sensitivity analysis would require comparing the outcome of hundreds of experimental protocols, which is both expensive and time-consuming. However, *in silico* modelling can be used to simulate a wide array of experiments, greatly decreasing the costs and time of the parameter sensitivity analysis.

This paper aims to provide a guide for the selection of the most efficient testing protocols for the characterization of material parameters for *in silico* modelling of hydrogel constructs and cartilage explants, with a minimum number of tests but maximum identifiability of the material parameters. To this end, we present, to the authors' knowledge, the first systematic FE-based parameter sensitivity analysis of the testing protocols to the material parameters of relevant constitutive models for hydrogels and cartilage. We focus on unconfined compression testing as it allows including lateral sample displacement (measured using optical techniques) together with measured reaction force as experimental measures into the sensitivity analysis (DiSilvestro and Suh, 2001). As an outcome, we provide a blueprint for experimentalists to optimize their mechanical testing protocols to ensure reliable experimental data collection of the relevant material parameters required for *in silico* models of cartilage and hydrogel constructs. Furthermore, the developed methodological framework is sufficiently generic so that it can be applied for the optimization of the mechanical characterization of other biological tissues.

2. Methods

2.1. Material model

2.1.1. Constitutive modelling of the hydrogel construct

The hydrogel construct was modelled as a homogenous porohyperelastic material. The hydrogel was assumed to be composed of a compressible porohyperelastic solid matrix saturated with an incompressible fluid that can be exuded from or absorbed into the porous solid matrix. The stress in the porohyperelastic material was estimated using an effective stress concept that couples the behaviour of the solid and fluid phases (Zahedmanesh et al., 2014):

$$\boldsymbol{\sigma}_h = \boldsymbol{\sigma}_{sm} - p\mathbf{I}, \tag{1}$$

where $\boldsymbol{\sigma}_h$ is the Cauchy stress tensor caused by external loading applied to the hydrogel, $\boldsymbol{\sigma}_{sm}$ is the Cauchy stress tensor of the solid matrix, p is the isotropic pore fluid pressure and $\mathbf{I}$ is the identity tensor.

The solid matrix was modelled with a neo-Hookean hyperelastic material:

$$\boldsymbol{\sigma}_{sm} = K_{sm}\frac{\ln(J)}{J}\mathbf{I} + \frac{G_{sm}}{J}\left(\mathbf{F}\mathbf{F}^T - J^{\frac{2}{3}}\mathbf{I}\right), \tag{2}$$

where $\mathbf{F}$ is the deformation gradient tensor and J is the determinant of $\mathbf{F}$. K_{sm} and G_{sm} are the bulk and shear moduli of the solid matrix, respectively, which are functions of Young's modulus (E_{sm}) and Poisson's ratio (ϑ_{sm}) of the solid matrix:

$$K_{sm} = \frac{E_{sm}}{3(1-2\vartheta_{sm})} \tag{3}$$

$$G_{sm} = \frac{E_{sm}}{2(1+\vartheta_{sm})} \tag{4}$$

The pore pressure is obtained using Darcy's law (Holmes and Mow, 1990):

$$q = -k\nabla p, \tag{5}$$

where q is referred to as the effective fluid velocity, k is the permeability of the material and ∇p is the pore fluid pressure gradient.

Summarized, the porohyperelastic material model contains three unknown material parameters (E_{sm}, ϑ_{sm} and k).

2.1.2. Constitutive modelling of the cartilage explant

The cartilage explant was modelled as a fibril-reinforced poroelastic (FRPE) material (Ebrahimi et al., 2019) composed of a porohyperelastic non-fibrillar matrix saturated with an incompressible fluid that can be exuded from or absorbed into the non-fibrillar matrix. The non-fibrillar matrix was reinforced with 4 primary collagen fibril families organized in an arcade-like pattern (Wilson et al., 2005b) and 13 randomly oriented secondary collagen fibril families.

The stress in the cartilage was estimated as:

$$\boldsymbol{\sigma}_c = \boldsymbol{\sigma}_{nf} + \boldsymbol{\sigma}_f - p\mathbf{I}, \tag{6}$$

where $\boldsymbol{\sigma}_c$ is the total Cauchy stress tensor in the material, $\boldsymbol{\sigma}_{nf}$ is the stress tensor of the non-fibrillar matrix and $\boldsymbol{\sigma}_f$ is the stress tensor of the fibrillar network.

The stress in the non-fibrillar matrix was estimated using a Neo-Hookean hyperelastic material model:

$$\boldsymbol{\sigma}_{nf} = K_{nf}\frac{\ln(J)}{J}\mathbf{I} + \frac{G_{nf}}{J}\left(\mathbf{F}\mathbf{F}^T - J^{\frac{2}{3}}\mathbf{I}\right), \tag{7}$$

where the bulk and shear modulus can be expressed in terms of Young's modulus (E_{nf}) and Poisson's ratio (ϑ_{nf}):

$$K_{nf} = \frac{E_{nf}}{3(1-2\vartheta_{nf})} \tag{8}$$

$$G_{nf} = \frac{E_{nf}}{2(1+\vartheta_{nf})} \tag{9}$$

The fibrillar network was assumed not to resist compression and to have a non-linear stress-strain behaviour in tension. This model was chosen due to its ability to simulate the mechanical behaviour of human tibial cartilage (Ebrahimi et al., 2019).

$$\begin{cases} \sigma_f = 0 \quad if\ \varepsilon_f \le 0 \\ \sigma_f = \frac{1}{2}E_f^{\varepsilon}\varepsilon_f^2 + E_f^0\varepsilon_f \ if\ \varepsilon_f > 0 \end{cases}, \tag{10}$$

where σ_f and ε_f are stress and strain in the fibril families and E_f^{ε} and E_f^0 are the strain-dependent and initial fibril network moduli, respectively. The stress in the fibrillar network was calculated as the sum of the stresses in the primary and secondary fibrils (Orozco et al., 2018):

$$\begin{cases} \sigma_{f,p} = \rho_z C\sigma_f \\ \sigma_{f,s} = \rho_z\sigma_f \end{cases}, \tag{11}$$

where $\sigma_{f,p}$ and $\sigma_{f,s}$ are the stresses in the primary and secondary fibrils, respectively. C is the ratio between primary and secondary fibril density, which was set to 12.16 and ρ_z is the depth-dependent relative collagen density, which was calculated as a function of normalized distance from the surface of the cartilage explant z (surface = 0, bottom = 1) (Wilson et al., 2004; Eskelinen et al., 2019):

$$\rho_z = 1.4z^2 - 1.1z + 0.59 \tag{12}$$

The stress tensor of the fibrillary network can then be written as:

$$\boldsymbol{\sigma}_f = \sum_{i=1}^{totf}\sigma_{f,i}\vec{e_f}\otimes\vec{e_f}, \tag{13}$$

where *totf* is the total number of fibril families, $\sigma_{f,i}$ is the stress in the primary and secondary fibrils, $\vec{e_f}$ is the fibril orientation vector and $\otimes$ denotes the outer product.

The pore pressure was calculated using Darcy's law (Eq. (5)), while permeability was assumed to be void ratio-dependent:

$$k = k_0\left(\frac{1+e}{1+e_0}\right)^M, \tag{14}$$

where k and k_0 denote current and initial permeability and e and e_0 denote current and initial void-ratio and M is the permeability void-ratio dependency constant. The initial void-ratio was set to 3 (Ebrahimi et al., 2019).

Summarized, the FRPE material model contains six unknown material parameters (E_{nf}, ϑ_{nf}, E_f^{ε}, E_f^0, k_0 and M).

2.2. Finite element model of hydrogel construct and cartilage explant

The FE models were constructed in Abaqus/CAE (V2017, Dassault Systèmes Simulia Corp., Johnston, RI) and, as detailed in section 2.1, different constitutive models were employed to simulate the behaviour of hydrogel constructs and cartilage explants.

Hydrogel constructs and cartilage explants were modelled as cylinders with dimensions comparable to the typical dimensions used in our bioreactor set-up (hydrogel constructs: diameter and height of 8 mm, cartilage explants: diameter and height of 4 mm). Since hydrogel was modelled as a homogeneous isotropic material the model geometry was constructed in an axisymmetric manner (Fig. 1a). As we wanted to implement the 3D collagen fibrils orientations in addition to their depth-wise content, the cartilage geometry was constructed in 3D (Fig. 1b) and modelled as FRPE material.

The hydrogel samples were meshed by 512 linear axisymmetric pore pressure continuum elements (element type CAX4P). The cartilage samples were meshed by 5508 linear pore pressure continuum elements (element type C3D8P). Mesh convergence was ensured by modelling both hydrogel construct and cartilage explant using half, twice and four times of the selected element numbers. The reaction force and maximum lateral displacement in the models were verified as convergence parameters.

Boundary conditions were applied as shown in Fig. 1a and b: the bottom nodes were fixed in the vertical direction (y-direction) and were free to move in the horizontal directions (x and z directions). A zero pore pressure (free fluid flow) was assigned to the nodes of the lateral surface of the cylinder. The nodes of the top surface were subjected to a compressive strain in the vertical direction, while they were free to move in the horizontal direction.

The compressive strain was applied according to three loading regimes: ramp loading, ramp loading followed by 15 min of relaxation and 10 cycles of dynamic loading (Fig. 1c) with different strain levels and rates (Table 1). The different loading protocols were chosen based on the experimental guide provided by Patel et al. (2019). The relaxation time was chosen based on the required time for the models of both hydrogel and cartilage to reach an equilibrium. In the case of the 10-cycle dynamic loading, the height of the sample may decrease after each loading cycle due to fluid exudation. To avoid this, a pre-compression of 5% strain was applied to the samples before applying the dynamic loading.

To assess the effect of extremely low or high loading rates on mechanical characterization of hydrogel constructs and cartilage explants, in addition to the loading protocols given in Table 1, the following loading protocols were analysed:

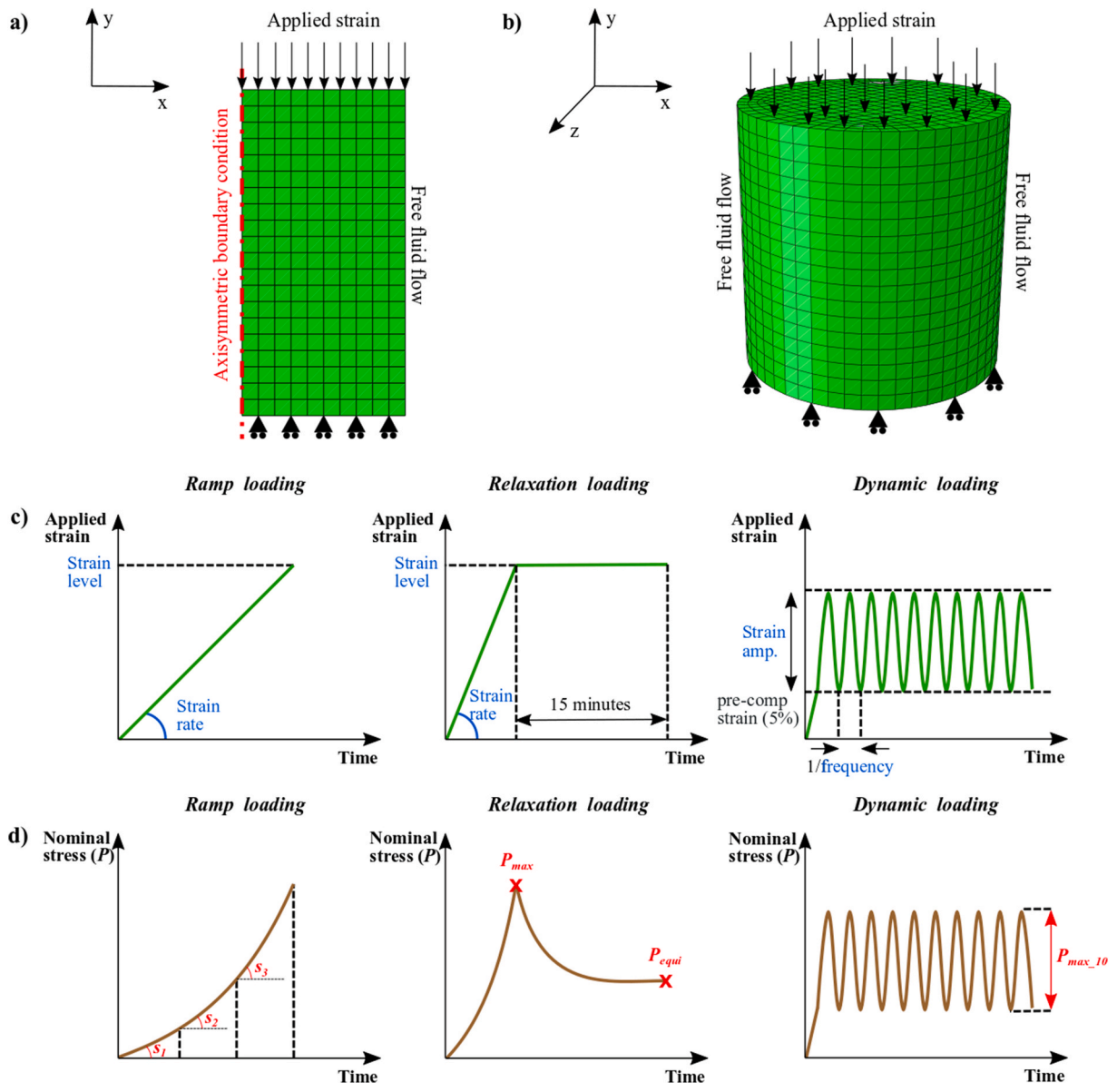

Fig. 1. Mesh and boundary conditions of a) hydrogel construct and b) cartilage explant models. c) Applied strain-time curves of the 3 loading regimes and the studied loading parameters in the FE simulations (blue parameters: detailed in Table 1). d) Examples of the obtained nominal stress-time curves from each of the 3 loading regimes and FE simulation target outputs studied in the parameter sensitivity analysis (red outputs, s_1,s_2 *and* s_3: the average slope of the nominal stress vs. time curve at three equally distributed zones of the ramp loading. P_{max} and P_{equi}: the nominal stress at the maximum point and at the end of the 15 min relaxation, P_{max_10}: the maximum nominal stress at the tenth cycle). The mean slopes in the relaxation loading are the same as the ramp loading.

- Dynamic loading of the hydrogel construct with 15% of strain at a relatively low frequency of 0.001 Hz.
- Ramp loading of the cartilage explant with 20% of strain at a relatively low strain rate of 0.001%/sec.
- Ramp loading of the cartilage explant with 20% of strain at a relatively too high rate of 100%/sec.

We did not test strain levels exceeding 20% as increasing the strain level in the mechanical characterization tests will cause cartilage and hydrogel sample damage and result in inaccurate mechanical characterization (Patel et al., 2019).

2.3. Parameter sensitivity analysis method

For both the hydrogel and cartilage sample and each loading protocol given in Table 1, a parameter sensitivity analysis was performed. In each of these parameter sensitivity analyses, the material parameters of the FE model were varied using a design of experiments method, adapted from (Elahi, 2018; Frauziols et al., 2016). The sensitivity of the FE model responses to the material parameters can then be used to determine the identifiable material parameters for each of the unconfined compression testing protocols of Table 1. The loading protocol that yields the highest sensitivity to the material parameters can be considered as the ideal protocol for material parameter characterization.

2.3.1. Input parameters

The material parameters of the porohyperelastic and FRPE material models were the input parameters for the parameter sensitivity analyses of the hydrogel constructs and cartilage explants, respectively. To compare the sensitivities, the material parameters were normalized and centred from −1 to 1 in their ranges (Table 3 and Table 4). In literature, a variety of mechanical properties has been reported for hydrogel

Table 1
Specifications of the different compressive loadings applied on the top surface of the cylindrical hydrogel and cartilage samples.

Loading regime	Loading parameters	
	Strain level (% of the sample initial height)	Strain rate/ frequency
Ramp	10	1%/sec
	20	1%/sec
	20	10%/sec
Ramp + 15 min relaxation	10	1%/sec
	20	1%/sec
	20	10%/sec
10-cycle dynamic	5% pre-compression+5% of amplitude	1 Hz
	5% pre-compression+15% of amplitude	1 Hz
	5% pre-compression+15% of amplitude	0.1 Hz

Table 2
Ranges of the hydrogel material parameters used in the parameter sensitivity analysis.

Material parameter	The minimum value of the range	The maximum value of the range
E_{sm}	0.02 MPa	0.08 MPa
ϑ_{sm}	0.1	0.4
k	1×10^{-12} $m^4N^{-1}s^{-1}$	4×10^{-12} $m^4N^{-1}s^{-1}$

Table 3
Ranges of the cartilage material parameters used in the parameter sensitivity analysis.

Material parameter	The minimum value of the range	The maximum value of the range
E_{nf}	0.3 MPa	0.9 MPa
ϑ_{nf}	0.15	0.45
E_f^e	10 MPa	30 MPa
E_f^0	0.3 MPa	0.9 MPa
k_0	0.6×10^{-15} $m^4N^{-1}s^{-1}$	1.8×10^{-15} $m^4N^{-1}s^{-1}$
M	2	6

Table 4
Uncertainty of the material parameters obtained through an inverse identification of the hydrogel construct using different testing protocols and in comparison with a known random set of material parameters. The uncertainty is expressed in terms of percentage difference from the corresponding ground truth parameter. The testing protocol with an asterisk is the optimal testing protocol based on the parameter sensitivity analysis.

Testing protocol	Measured outputs	Uncertainty in the identification of material parameters (%)		
		E_{sm}	ϑ_{sm}	k
*Relaxation loading (20% strain-10%/sec)	$RF + LD$	0.01	0.21	1.40
Relaxation loading (20% strain-10%/sec)	RF	1.11	31.19	21.00
Ramp loading (20% strain-10%/sec)	$RF + LD$	8.18	42.6	12.14
10 cycle dynamic loading (5% pre-compression +15% of amplitude)	$RF + LD$	5.08	25.15	34.25

constructs (Nguyen et al., 2009b; Matyash et al., 2014; Kaklamani et al., 2014; Julian et al., 1988). The material parameter ranges for the hydrogel construct were selected based on mechanical characterization results of Alginate hydrogel (Nguyen et al., 2009b; Kaklamani et al., 2014), whereas the ranges for the cartilage explant were selected based on previous mechanical characterization of healthy human tibial cartilage (Ebrahimi et al., 2019).

2.3.2. Design of experiments method

For each parameter sensitivity analysis, a set of FE simulations was defined using a full factorial design of experiments with interactions between pairs of the varied material parameters. This resulted in 2^m (m being the number of varied material parameters, *i.e.* 3 for hydrogels and 6 for cartilage) simulations that covered the maximum and minimum values of the parameters (Table 2 and Table 3) plus a simulation at the centre of the ranges. Therefore, in total n number of simulations were performed for each analysis:

$$n = 2^m + 1, \tag{15}$$

where $n = 9$ for the hydrogel simulations and $n = 65$ for the cartilage simulations.

2.3.3. Selection of outputs from the FE simulations

Two results at different instants of the loading procedure were taken from the FE simulations: (i) the reaction force $(RF(t))$ at the bottom surface of the cylindrical sample and (ii) the lateral displacement $(LD(t))$ at the middle node of the lateral surface of the cylinder. The nominal stress $P(t)$ can be derived from $RF(t)$, by dividing it by the initial cross-section area of the cylinder. These variables were used to define the outputs for the three loading regimes (shown in Fig. 1d):

- Four outputs were defined for ramp loading: The average slope of the nominal stress vs. time curve at three equally distributed zones (s_1, s_2 and s_3)and the lateral displacement at the maximum applied strain (LD_{max}).
- Three outputs were defined for relaxation loading: The nominal stress at the maximum point (P_{max})and at the end of the 15 min relaxation (P_{equi}), and the lateral displacement at the end of the relaxation (LD_{equi}). Note, that a relaxation loading is always preceded by a ramp loading, hence s_1, s_2 and s_3 were also obtained.
- Two outputs were defined for dynamic loading: The maximum nominal stress at the tenth cycle (P_{max_10})and lateral displacement at the time when the maximum strain was applied in the tenth cycle (LD_{max_10}).

2.3.4. Definition of approximating function

A first-order polynomial response surface including interactions between pairs of the material parameters (x_i) was fitted on the output values obtained from n (Eq. (15)) FE simulations. The fitted functions are obtained as (Elahi, 2018; Frauziols et al., 2016):

$$Y_{approx} = \beta_0 + \sum_{i=1}^{m} \beta_i \times x_i + \sum_{\substack{i,j=1 \\ j>i}}^{m} \beta_{ij} \times x_i \times x_j, \tag{16}$$

where Y_{approx} is the approximated output parameter using the fitted surface to the outputs of FE simulations, β_0 is the average of outputs obtained from the FE simulations, m is the number of material parameters and β_i and β_{ij} are the sensitivity coefficients of the material parameters and their interactions in the fitted function, respectively. To compare the sensitivity of the FE simulation outputs to each of the material parameters, these coefficients (β_i and β_{ij}) were normalized by the average output (β_0). The absolute value of the normalized coefficients represents the sensitivity of the FE simulation output to the corresponding parameters. The higher the absolute value of the coefficient, the more sensitive the FE model output to a change in this material parameter. The positive and negative values of the coefficients show the direct and inverse relationship between the studied output and the parameter, respectively. The higher the absolute value of β_i, the better

the identifiability of the corresponding material parameter x_i . In other words, a loading protocol that yields the highest absolute values of β_i, will yield the most reliable material parameters during an inverse identification process of an experiment that uses that specific loading protocol (see Fig. 2). We will refer to this loading protocol as the optimal testing protocol.

2.4. Inverse identification verification method

The results of the performed parameter sensitivity analysis were used to provide a guide for the selection of the optimal testing protocols for the mechanical characterization of hydrogel constructs and cartilage explants.

2.4.1. Numerical verification method

Since there is no ground truth for the validation of the obtained mechanical properties based on the inverse characterization of hydrogel constructs and cartilage explants, a numerical verification is used. This 3-step numerical verification determines the uncertainty during inverse identification and quantifies the improvements made by the proposed testing protocols in the following steps:

1. FE simulations for both the hydrogel construct and the cartilage explant were performed with the optimal testing protocol as described in the previous section and using a known set of material parameters, within the ranges given in Tables 2 and 3. The results of these simulations (*RF(t)* and *LD(t)*), were used as virtual experimental data. Next, an inverse identification procedure (Elahi et al., 2019) was performed starting with random initial guesses for the material parameters.
2. The same process is repeated but now with conventional testing protocols suggested in the literature (Patel et al., 2019). Besides, the effect of having no access to the lateral displacement ($LD(t)$) as an experimental output on the uncertainty in inverse identification was studied by using only reaction force (*RF(t)*) as the output of experiment in one testing group.
3. The errors of the resulting material parameters from steps 1 and 2 with respect to the known material parameters used in the virtual experiments were calculated and compared.

2.4.2. Inverse identification method

The material parameters of both porohyperelastic constitutive model (E_{sm}, ϑ_{sm} and k of hydrogel constructs) and FRPE constitutive model (E_{nf}, ϑ_{nf}, E_f^c, E_f^0, k_0 and M of cartilage explants) were obtained using an inverse identification method. This method optimizes the reaction force-time-response and maximum lateral displacement-time-response (*RF(t)* and *LD(t)*) of the models to the corresponding results of the experiments (virtual experiments in this paper). The optimization was performed using the Nelder-Mead simplex algorithm (*fminsearch* in Matlab R2018b) (Nelder and Mead R, 1965). The normalized mean square error between the simulation and experimental results was used as the objective function in the optimization algorithm:

$$OF = \frac{1}{l}\sum_{i=1}^{l}\left(\frac{RF_i^{sim} - RF_i^{exp}}{RF_i^{exp}}\right)^2 + \frac{1}{k}\sum_{j=1}^{k}\left(\frac{LD_j^{sim} - LD_j^{exp}}{LD_j^{exp}}\right)^2, \quad (17)$$

where RF_i^{sim} and RF_i^{exp} are simulated and experimental reaction force values, LD_j^{sim} and LD_j^{exp} are simulated and experimental lateral displacement values, l is the total number of reaction force data points and k is the total number of lateral displacement data points. The Matlab script of the optimization procedure is provided as supplementary material (section S3).

3. Results

The results of the parameters sensitivity analysis are detailed in the supplementary materials (section S1, Figs. S1–S8). In the following paragraphs, the optimal testing protocols selected based on the aforementioned analysis, are presented, after which it is shown how the results of the inverse identification validate the selected protocols.

3.1. Hydrogel construct

3.1.1. Selection of optimal testing protocol

The parameter sensitivity analysis results show that the output parameters of a relaxation loading protocol with 20% strain level and 10%/sec strain rate (Fig. 3a) are highly sensitive to all three material parameters: $P_{max}$and $P_{equi}$are highly dependent on E_{sm} (Figs. S1a and

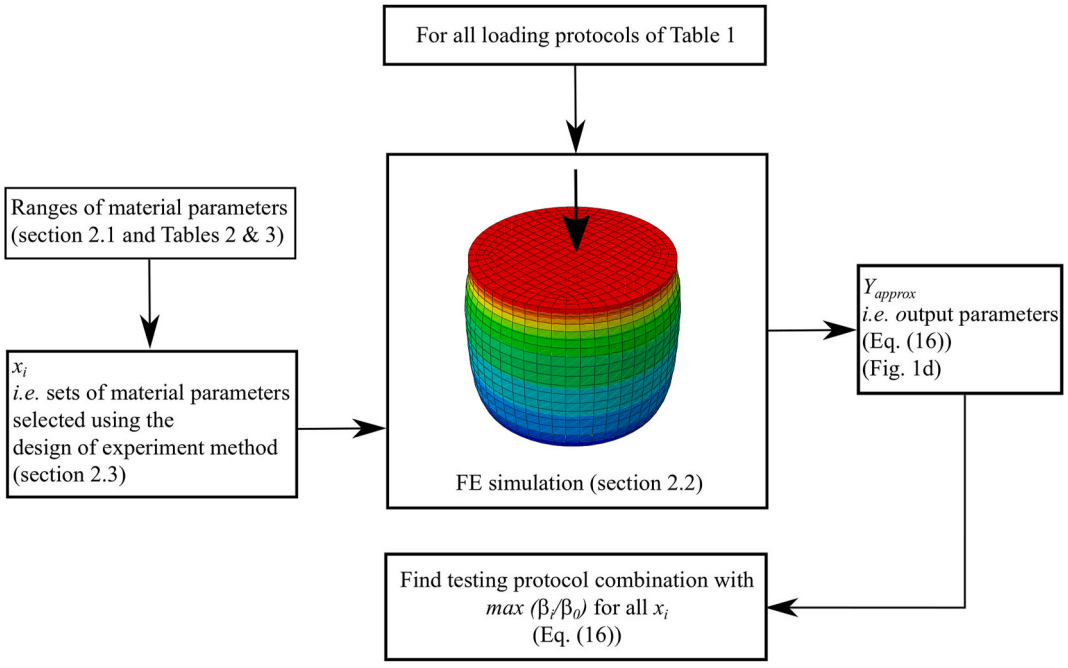

Fig. 2. Workflow to determine the optimal loading protocols for mechanical characterization of hydrogel constructs and cartilage explants.

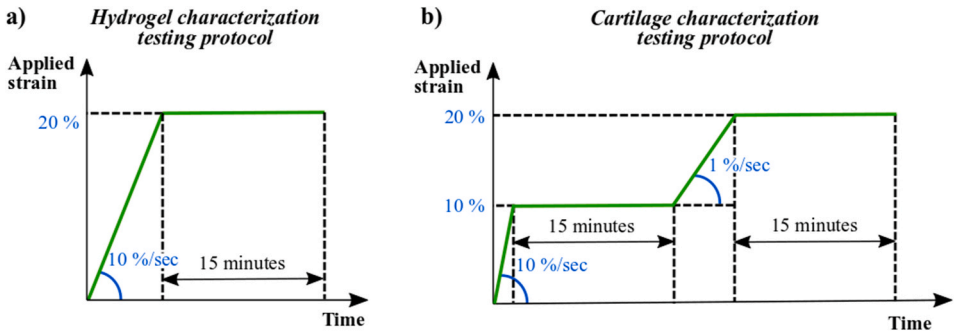

Fig. 3. Optimal testing protocols based on the parameter sensitivity analysis for inverse identification of material parameters of a) the porohyperelastic material model for hydrogel constructs and b) the FRPE material model for cartilage explants. Strains are in percentage of the sample initial height (nominal strain).

S1b), $LD_{max}$is highly dependent on all three material parameters (Fig. S1a) and $LD_{equi}$is highly dependent on ϑ_{sm} (Fig. S1b).

Dynamic loading provides similar dependencies to the material parameters as ramp and relaxation loading, depending on the loading frequency (compare Figs. S4a and S4c to Figs. S1a and S1b). Since performing dynamic loading tests requires more specific loading devices than performing ramp and relaxation loadings, the optimal testing protocol was chosen as a combination of ramp and relaxation loadings.

3.1.2. Inverse identification verification

The uncertainty of the identified material parameters of the hydrogel construct using different testing protocols are compared in Table 4. For each loading regime, only the testing protocol with minimum identification uncertainty is given in Table 4. The optimal testing protocol identified the material parameters of the porohyperelastic constitutive model with very limited uncertainty (variation from true value $<$ 2%). Note that all the data points (in terms of *RF* and *LD)* were used in the inverse identification algorithm for optimization purpose (not only the studied output parameters in the parameter sensitivity analysis). To determine the effect of using *LD* as an additional experimental output from unconfined compression tests on mechanical characterization results, the material parameters were identified using only *RF* as test output in one of the test groups. The results show a considerable (about 30% and 20%) increase in uncertainty of identification of Poisson's ratio (ϑ_{sm}) and permeability parameter (k).

When repeating the inverse identifications using three different sets of known material parameters and for different initial guesses in the *fminsearch* optimization algorithm, the same ranges of uncertainties were obtained.

3.2. Cartilage explant

3.2.1. Choice of testing protocol

The parameter sensitivity analysis results suggest that the output parameters of a ramp loading test at low strain rate (1%/sec) and a relaxation test are highly sensitive to the non-fibrillar matrix parameters (E_{nf} and ϑ_{nf} – Figs. S5a and S5c). The output parameters of ramp loading at a higher rate (10%/sec) are significantly sensitive to the fibril parameters (E_f^e and E_f^0) and the initial permeability (k_0 – Fig. S5b). Using these results, a two-step ramp plus relaxation loading protocol at different loading rates (Fig. 3b), while measuring both *RF* and *LD*, provides maximum sensitivity to the different parameters. Since compressive strain levels over 20% have been reported to cause defects in the cartilage tissue (Orozco et al., 2018; Hosseini et al., 2014), each of the two steps of the proposed optimal protocol (Fig. 3b) is limited to 10% compressive strain. Besides, according to the parameter sensitivity analysis results (supplementary materials), the dependency of output parameters of the ramp loading on the material parameters had the same trend for the 20% and 10% compressive strain tests. Furthermore, we propose to apply the higher loading rate in the first step since this higher loading rate causes more reaction force within the sample, which may cause defects in the tissue at higher strain levels.

- Inverse identification verification

The same numerical verification as the hydrogel construct (section 3.1) was used to validate the selected optimal testing protocol for the cartilage explant (Fig. 3b). The uncertainty of the identified material parameters of the cartilage explant using different testing protocols are compared in Table 5. For each loading regime, only the testing protocol with minimum identification uncertainty is given in Table 5. The proposed optimal testing protocol resulted in the lowest uncertainty (variation from true value $<$ 6%) compared to other loading protocols. Besides, the results show an increase in uncertainty of material identification (especially for permeability parameters k_0 and M with about 22% and 26% increase, respectively) by removing lateral displacement from experimental outputs.

4. Discussion

4.1. Relevance of the study

Finite element (FE) models of bioreactor setups for cell-seeded hydrogels or of human cartilage are used to identify the local mechanical environment of the constructs or tissue, which can bring insight into mechanoregulated degenerative or regenerative processes. For instance, FE studies have shown that proteoglycan loss in mechanically injured articular cartilage is controlled by maximum shear strain, deviatoric strain and fluid velocity within the cartilage (Orozco et al., 2018). Another study showed that chondrogenesis in cell-seeded hydrogels is controlled by compressive principal strains within the constructs (Zahedmanesh et al., 2014). Several adaptive cartilage degradation and regeneration algorithms are proposed in the literature (Mukherjee et al., 2020; Hendrikson et al., 2017). These can only be translated to realistic FE models if the material parameters are accurately identified, which highlights the importance of this study.

Different experimental methods with various loading protocols have been used in literature to identify material parameters of hydrogel constructs and cartilage explants through inverse mechanical characterization (Patel et al., 2019). However, there is limited insight into the degree to which these testing protocols yield accurate material parameters, suitable for subsequent FE modeling. An experimental protocol must allow unique identification of each parameter with a minimum of uncertainty. This usually entails a combination of tests with different sensitivities to the different material parameters. In the present study, we derived optimal mechanical testing protocols for accurate characterization of hydrogel constructs and cartilage explants, shown in Fig. 3. To enable broad applicability, we focused on unconfined compression testing with and without optical measurement of the lateral displacement, which is a relatively simple testing procedure available in many

Table 5
Uncertainty of the material parameters obtained through inverse identification of the cartilage explant using different testing protocols and in comparison with a known random set of material parameters. The uncertainty is expressed in terms of percentage difference from the corresponding ground truth parameter. The testing protocol with an asterisk is the optimal testing protocol based on the parameter sensitivity analysis.

Testing protocol	Measured outputs	Uncertainty in the identification of material parameters (%)					
		E_{nf}	ϑ_{nf}	k_0	M	E_f^0	E_f^e
* 2-step relaxation loading (10% strain-10%/sec) (10% strain-1%/sec)	$RF + LD$	1.31	1.84	2.96	5.74	1.36	1.45
2-step relaxation loading (10% strain-10%/sec) (10% strain-1%/sec)	RF	2.12	2.67	25.36	31.25	6.32	5.36
Ramp loading (20% strain-10%/sec)	$RF + LD$	5.21	4.36	28.69	42.23	5.37	7.35
Relaxation loading (20% strain-10%/sec)	$RF + LD$	4.36	6.34	49.32	62.21	11.14	15.87
10 cycle dynamic loading (5% pre-compression +15% of amplitude)	$RF + LD$	7.98	9.12	30.65	40.98	8.54	5.12

research groups.

4.2. Parameter sensitivity analysis

4.2.1. Hydrogel construct

The permeability (k) has a limited effect on the reaction force output for all loading regimes (ramp, relaxation, dynamic loading). This is because the fluid exudation in the saturated porous materials is a time-dependent process. The tested loading rates might not have been small enough to allow fluid exudation. We verified this by performing sensitivity analysis of dynamic loading with 15% of strain at a relatively low frequency of 0.001 Hz (data in the supplementary materials, Fig. S4d). This increased the dependency of the nominal stress at the 10th cycle of loading (P_{max_10}) on k by around 190% in comparison to the minimum frequency considered (0.1 Hz in Table 1, for the dependency of P_{max_10} to k at this frequency, see Fig. S4c). Therefore, to increase the identifiability of k from the measured reaction force in dynamic loading, lower loading frequencies are advisable.

On the other hand, the effect of k can be observed on the maximum lateral displacement obtained from the ramp and dynamic loadings (LD_{max}), indicating the importance of measuring this lateral displacement during an experiment. Therefore, including LD measurement as an experimental output includes the effect of k in the test results. Fig. S1a shows an inverse relationship between LD_{max} and k, since an increase in fluid pressure and, consequently, more lateral bulging is expected for a smaller k. This effect was far less at the end of relaxation loading (LD_{equi}), shown in Fig. S1b, because the fluid exudation stops at the equilibrium point and the response of the material is only due to the solid constituents. At this point, the horizontal displacement is prominently dependent on ϑ_{sm}. As a consequence, k has maximum identifiability by measuring LD_{max} at the end of ramp loading, while ϑ_{sm} can be identified with less uncertainty by measuring LD_{equi} at the end of relaxation loading.

The inverse identification verification results (Table 4) showed that Young's modulus of the solid matrix (E_{sm}) can be identified with small uncertainty using any of the loading protocols. In agreement with the results of our parameter sensitivity analysis, identification uncertainties of the Poisson's ration of the solid matrix (ϑ_{sm}) and material permeability (k) were lowest for the tests where the lateral displacement was measured.

4.2.2. Cartilage explant

The dependency of the reaction stress parameters (red parameters in Fig. 1d) on the non-fibrillar matrix modulus and Poisson's ratio (E_{nf} and ϑ_{nf}) and fibril moduli (E_f^0 and E_f^e) in all the loading protocols were relatively dominant. This guaranteed the influence of these parameters on the test outputs, which shows the identifiability of these parameters through inverse identification using the test outputs.

The Poisson's ratio and modulus of the matrix (E_{nf} and ϑ_{nf}) have a significant effect on the output parameters of ramp loading at low strain rates (Fig. S5a). At higher strain rates, the fibril moduli (E_f^0 and E_f^e) dominate. This is in agreement with findings of Quiroga et al. (2017). Wilson et al. (2005b) observed that in ramp loading with a strain of 5% or lower, the fibers are not stretched and the response is mostly due to the non-fibrillar matrix. To evaluate this effect, we additionally studied the sensitivity of ramp loading with a 5% strain level and a 1%/sec strain rate on the material parameters. The obtained results had the same trend as the parameter sensitivity analysis results shown in Fig. S5a (ramp loading with 20% strain level and 1%/sec strain rate). We, therefore, conclude that within the tested ranges, strain rate is more important than strain amplitude to allow distinction between the constituents. Thereby, if the strain level is in a safe range that does not cause an injury to the tissue, selection of an optimized strain rate would increase the identifiability of the material parameters of cartilage tissue.

The dependency on the permeability parameters (k_0 and M) is low to non-existent for all of the loading protocols (Fig. S5a). According to literature, decreasing the strain rate to 0.001%/sec would increase the effect of the permeability on the reaction stress (Olvera et al., 2015; DiSilvestro and Suh, 2001). This was evaluated by performing a sensitivity analysis on the unconfined compression ramp loading with the 20% strain level and a very small 0.001%/sec strain rate (see Fig. S6b). However, no increase in dependency was observed. This can be due to the narrow range selected for the permeability parameters in this study (Table 3). The range for these parameters can be much wider, especially for OA cartilage (Ebrahimi et al., 2019).

Still, a ramp loading at 10%/sec strain rate is an optimal protocol among the variations studied within this research. Increasing the strain rate from 1%/sec to 10%/sec in the ramp loading increased the effect of permeability parameters on both reaction stress and maximum horizontal displacement, relatively (compare Figs. S5a and S5b). This results in a better identifiability of permeability parameters at 10%/sec strain rate. To see the effect of higher strain rates on the dependency of the tests on the permeability parameters, another sensitivity analysis was performed on ramp loading with 20% strain level and 100%/sec strain rate (Fig. S6c). Interestingly, the high strain rate caused a reduction of dependency on the permeability parameters compared with the 10%/sec strain rate (compare Figs. S5b and S6c).

According to the inverse identification verification results (Table 5), a two-step relaxation loading protocol effectively increases the accuracy of material parameter identification. Based on these results (Table 5) and confirm the results of the parameter sensitivity analysis, the uncertainties in the identification of matrix and fibril parameters were small. On the other hand, the low dependency of the experimental results on the permeability parameters increases the uncertainty of their inverse identification (Table 5). Nonetheless, by measuring the horizontal displacement of the sample, we can decrease this uncertainty.

Each of the proposed mechanical characterization testing protocols needs to be preceded by a preload step to ensure contact between the loading plate and the sample. The applied preload needs to be small compared to the maximum load applied during the test (we propose less than 5% of the maximum load). This preload has to be followed by a relaxation until the measured reaction force becomes stable. Then a

sinusoidal strain with a small amplitude compared to the maximum load applied during the test (*e.g.* less than 5% of the maximum load) has to be applied to the sample and recovered back to the preload to ensure a stable initial condition. At this point, the force and displacement must be the same as they were initially after applying the preload.- *Using the developed method for mechanical characterization of other biological tissues*.

Mechanical characterization of biological tissues is a challenging but essential task for understanding their mechanical behaviour and developing *in silico* frameworks. The most important step in mechanical characterization is defining proper testing protocols and measuring those outputs that are sensitive to variations in mechanical properties of the tissues. To this end, the developed systematic parameter sensitivity analysis in this paper can be adapted for other biological tissues by using their specific constitutive models and testing protocols that are commonly used for their characterization. Moreover, the potential of newly designed testing protocols for reliable mechanical characterization of biological tissues can be assessed using the method developed in this paper.

4.2.3. Limitations

There are some limitations to the current study, summarized below:

- The goal of this paper was to suggest experimental protocols that can be performed at any typical mechanical laboratory with a uniaxial testing device, allowing to obtain the best possible results in terms of the material parameters of established constitutive models of articular cartilage tissue and hydrogel constructs. It is known that the existing constitutive models face convergence difficulties when wider ranges of material parameters are used, which limits the range of material parameters that could be included in the present study. This limitation must be addressed by improving the constitutive models, which is out of the scope of this study. Therefore, the validity of the proposed protocols to study damaged cartilage or hydrogels with mechanical properties well outside the range evaluated here needs to be considered with caution. The results of this paper are therefore valid for a selected range of values of the parameters, relevant for healthy human tibial cartilage and hydrogels. These ranges were selected using the results of mechanical characterization performed in literature. A different parameter range can change the dependency of the outputs on that parameter. Caution is needed when extrapolating our findings to other types of cartilage and hydrogels, whose material parameters can vary over a wide range depending on the species, age and location of cartilage samples or the different types of hydrogels.
- First-order polynomials with interaction between pairs of parameters were fitted to the results of the FE models. The ANOVA results ($R^2 > 0.99$) validate the quality of the approximated function. However, fitting a higher-order function may increase the agreement between the approximated function and FE simulation results.
- To perform the parameter sensitivity analysis, certain output parameters (*e.g.* average slope of nominal stress – time curve or maximum lateral displacement) had to be selected from the FE simulation results. Dependencies of the studied output parameters on the material parameters give an overview of the dependency of the whole output data. However, there is a possibility that the selection of other output parameters would reveal different dependencies on the material parameters. For instance, the phase lag between applied strain and reaction force in dynamic loading could be an interesting output parameter to study in addition to the studied output parameters in this paper.
- In this paper, several loading protocols for mechanical characterization of hydrogel constructs and cartilage explants were selected based on established experimental studies (Patel et al., 2019). They are therefore considered to be the most commonly used and most practically feasible. Nevertheless, other combinations of loading protocols, *i.e.* loading types, ranges and rates, could be tested using the same parameter sensitivity analysis method presented here, which might yield an even better loading regime for mechanical characterization of the samples.

5. Conclusion

This paper presented an *in silico* parameter sensitivity analysis to help identify the optimal experimental protocol for unconfined compression testing of hydrogel constructs and cartilage explants. For hydrogels, our analysis yielded a single step ramp loading followed by 15 min relaxation as the optimal protocol. For cartilage, a two-stepped ramp loading each followed by 15 min of relaxation was found. When using the experimental results of the proposed testing protocols in an inverse identification scheme, thereby including the measurement data of the lateral displacement, material parameters of the porohyperelastic (hydrogel) and fibril-reinforced poroelastic (cartilage) material models can be obtained with minimal uncertainty. Compared to conventional tests, an improvement of uncertainty in identified material parameters from 42% to 1% was obtained in this respect for hydrogels, and from 56% to 1% for cartilage. Although the proposed loading protocols are simple, measuring the lateral deformation of the samples in addition to the reaction force allows for a unique identification of the different material parameters. To Summarize, we suggest a simple loading protocol while analysing just one additional output (lateral deformation) which enables unique identification of the material parameters of state-of-the-art constitutive models of cartilage and hydrogel. Although the current study focused on unconfined compression for a relevant range of parameters representative for tibial cartilage, the proposed *in silico* framework can be expanded to other parameter ranges and hence other cartilage types as well as to other experimental test protocols.

CRediT authorship contribution statement

Seyed Ali Elahi: Conceptualization, Data curation, Formal analysis, Funding acquisition, Investigation, Methodology, Project administration, Software, Validation, Visualization, Writing – original draft, Writing – review & editing. **Petri Tanska:** Conceptualization, Methodology, Software, Writing – review & editing. **Satanik Mukherjee:** Conceptualization, Methodology, Software, Writing – review & editing. **Rami K. Korhonen:** Conceptualization, Methodology, Supervision, Writing – review & editing. **Liesbet Geris:** Supervision, Writing – review & editing. **Ilse Jonkers:** Conceptualization, Funding acquisition, Methodology, Project administration, Supervision, Writing – review & editing. **Nele Famaey:** Conceptualization, Funding acquisition, Methodology, Project administration, Supervision, Writing – review & editing.

Declaration of competing interest

The authors declare that they have no known competing financial interests or personal relationships that could have appeared to influence the work reported in this paper.

Acknowledgements

This work was supported by Marie Skłodowska–Curie Individual Fellowship (CREATION project: MSCA–IF–2019-893771) and KU Leuven/FWO Happy Joints project (C14/18/077 and G045320N). It is also part of the EOS excellence program Joint-Against OA (G0F8218N).

Appendix A. Supplementary data

Supplementary data to this article can be found online at https://doi.org/10.1016/j.jmbbm.2021.104795.

References

Ateshian, G.A., Hung, C.T., 2003. Functional properties of native articular cartilage. In: Guilak, F., Butler, D.L., Goldstein, S.A., Mooney, D.J. (Eds.), Functional Tissue Engineering. Springer, New York, pp. 46–68.

Ateshian, G.A., Rajan, V., Chahine, N.O., Canal, C.E., Hung, C.T., 2009. Modeling the matrix of articular cartilage using a continuous fiber angular distribution predicts many observed phenomena. J. Biomech. Eng.-T. Asme. 131, 061003.

Babalola, O.M., Bonassar, L.J., 2009. Parametric finite element analysis of physical stimuli resulting from mechanical stimulation of tissue engineered cartilage. J. Biomech. Eng.-T. Asme. 131, 061014.

Bandeiras, C., Completo, A., 2017. A mathematical model of tissue-engineered cartilage development under cyclic compressive loading. Biomech. Model. Mechanobiol. 16, 651–656, 66.

Beynnon, B.D., Fleming, B.C., Labovitch, R., Parsons, B., 2002. Chronic anterior cruciate ligament deficiency is associated with increased anterior translation of the tibia during the transition from non-weightbearing to weightbearing. J. Orthop. Res. 20, 332–337.

Brittberg, M., Lindahl, A., Nilsson, A., Ohlsson, C., Isaksson, O., Peterson, L., 1994. Treatment of deep cartilage defects in the knee with autologous chondrocyte transplantation. N. Engl. J. Med. 331, 889–895.

Danso, E.K., Julkunen, P., Korhonen, R.K., 2018. Poisson's ratio of bovine meniscus determined combining unconfined and confined compression. J. Biomech. 77, 233–237.

DiSilvestro, M.R., Suh, J.K., 2001. A cross-validation of the biphasic poroviscoelastic model of articular cartilage in unconfined compression, indentation, and confined compression. J. Biomech. 34, 519–525.

DiSilvestro, M.R., Zhu, Q., Wong, M., Jurvelin, J.S., Suh, J.K., 2001. Biphasic poroviscoelastic simulation of the unconfined compression of articular cartilage: I—simultaneous prediction of reaction force and lateral displacement. J. Biomech. Eng.-T. Asme. 123, 191–197.

Drury, J.L., Mooney, D.J., 2003. Hydrogels for tissue engineering: scaffold design variables and applications. Biomaterials 24, 4337–4351.

Ebrahimi, M., Ojanen, S., Mohammadi, A., Finnilä, M.A., Joukainen, A., Kröger, H., Saarakkala, S., Korhonen, R.K., Tanska, P., 2019. Elastic, viscoelastic and fibril-reinforced poroelastic material properties of healthy and osteoarthritic human tibial cartilage. Ann. Biomed. Eng. 47, 953–966.

Elahi, S.A., 2018. Towards In-Vivo and In-Situ Mechanical Characterization of Soft Living Tissues. PhD thesis. Grenoble Alpes University, Grenoble.

Elahi, S.A., Connesson, N., Payan, Y., 2018. Disposable system for in-vivo mechanical characterization of soft tissues based on volume measurement. J. Mech. Med. Biol. 18, 1850037.

Elahi, S.A., Connesson, N., Chagnon, G., Payan, Y., 2019. In-vivo soft tissues mechanical characterization: volume-based aspiration method validated on silicones. Exp. Mech. 59, 251–261.

Elahi, S.A., Fehervary, H., Famaey, N., Tanska, P., Korhonen, R.K., Jonker, I., 2020. Optimized multi-axial loading to enhance chondrogenesis and limit proteoglycan loss in cartilage explants during bioreactor experimentation. Osteoarthritis Cartilage 28, S519.

Eskelinen, A.S., Mononen, M.E., Venäläinen, M.S., Korhonen, R.K., Tanska P, P., 2019. Maximum shear strain-based algorithm can predict proteoglycan loss in damaged articular cartilage. Biomech. Model. Mechanobiol. 18, 753–778.

Evans, S., 2017. How can we measure the mechanical properties of soft tissues?. In: Material Parameter Identification and Inverse Problems in Soft Tissue Biomechanics. Springer Cham, pp. 67–83.

Farokhi, M., Jonidi Shariatzadeh, F., Solouk, A., Mirzadeh, H., 2020. Alginate based scaffolds for cartilage tissue engineering: a review. Int. J. Polym. Mater. 69, 230–247.

Frauziols, F., Chassagne, F., Badel, P., Navarro, L., Molimard, J., Curt, N., Avril, S., 2016. In vivo identification of the passive mechanical properties of deep soft tissues in the human leg. Strain 52, 400–411.

Hendrikson, W.J., Deegan, A.J., Yang, Y., Van Blitterswijk, C.A., Verdonschot, N., Moroni, L., Rouwkema, J., 2017. Influence of additive manufactured scaffold architecture on the distribution of surface strains and fluid flow shear stresses and expected osteochondral cell differentiation. Front. Bioeng. Biotech. 10, 6.

Holmes, M.H., Mow, V.C., 1990. The nonlinear characteristics of soft gels and hydrated connective tissues in ultrafiltration. J. Biomech. 23, 1145–1156.

Hosseini, S.M., Wilson, W., Ito, K., Van Donkelaar, C.C., 2014. A numerical model to study mechanically induced initiation and progression of damage in articular cartilage. Osteoarthritis Cartilage 22, 95–103.

Hosseini, S.A., Mohammadi, R., Noruzi, S., Ganji, R., Oroojalian, F., Sahebkar, A., 2021. Evolution of hydrogels for cartilage tissue engineering of the knee: a systematic review and meta-analysis of clinical studies. Joint Bone Spine 88, 105096.

Jacobi, M., Villa, V., Magnussen, R.A., Neyret, P., 2011. MACI-a new era? Sports Med. Arthrosc. Rehabil. Ther. Technol. 3.

Jones, B., Hung, C.T., Ateshian, G., 2016. Biphasic analysis of cartilage stresses in the patellofemoral joint. J. Knee Surg. 29, 92–98.

Julian, T.N., Radebaugh, G.W., Wisniewski, S.J., 1988. Permeability characteristics of calcium alginate films. J. Contr. Release 7, 165–169.

Kaklamani, G., Cheneler, D., Grover, L.M., Adams, M.J., Bowen, J., 2014. Mechanical properties of alginate hydrogels manufactured using external gelation. J. Mech. Behav. Biomed. 36, 135–142.

Kazemi, M., Li, L.P., 2014. A viscoelastic poromechanical model of the knee joint in large compression. Med. Eng. Phys. 36, 998–1006.

Kazemi, M., Dabiri, Y., Li, L.P., 2013. Recent advances in computational mechanics of the human knee joint. Comput. Math. Method M. 19, 1–27.

Kelly, D.J., Prendergast, P.J., 2006. Prediction of the optimal mechanical properties for a scaffold used in osteochondral defect repair. Tissue Eng. 12, 2509–2519.

Kisiday, D.J., Jin, M., DiMicco, M.A., Kurz, B., Grodzinsky, A.J., 2004. Effects of dynamic compressive loading on chondrocyte biosynthesis in self-assembling peptide scaffolds. J. Biomech. 37, 595–604.

Kundu, J., Shim, J.H., Jang, J., Kim, S.W., Cho, D.W., 2015. An additive manufacturing-based PCL–alginate–chondrocyte bioprinted scaffold for cartilage tissue engineering. J. Tissue Eng. Regen. M. 9, 1286–1297.

Li, L.P., Soulhat, J., Buschmann, M.D., Shirazi-Adl, A., 1999. Nonlinear analysis of cartilage in unconfined ramp compression using a fibril reinforced poroelastic model. Clin. Biomech. 14, 673–682.

Li, L., Yang, L., Zhang, K., Zhu, L., Wang, X., Jiang, Q., 2020. Three-dimensional finite-element analysis of aggravating medial meniscus tears on knee osteoarthritis. J. Orthop. Transl. 20, 47–55.

Matyash, M., Despang, F., Ikonomidou, C., Gelinsky, M., 2014. Swelling and mechanical properties of alginate hydrogels with respect to promotion of neural growth. Tissue Eng. C Methods 20, 401–411.

Mohammadi, H., Mequanint, K., Herzog, W., 2013. Computational aspects in mechanical modeling of the articular cartilage tissue. Proc. Inst. Mech. Eng. H. 227, 402–420.

Mononen, M.E., Tanska, P., Isaksson, H., Korhonen, R.K., 2016. A novel method to simulate the progression of collagen degeneration of cartilage in the knee: data from the osteoarthritis initiative. Sci. Rep. 6, 21415.

Mononen, M.E., Tanska, P., Isaksson, H., Korhonen, R.K., 2018. New algorithm for simulation of proteoglycan loss and collagen degeneration in the knee joint: data from the osteoarthritis initiative. J. Orthop. Res. 36, 1673–1683.

Mukherjee, S., Nazemi, M., Jonkers, I., Geris, L., 2020. Use of computational modeling to study joint degeneration: a review. Front. Bioeng. Biotech. 8, 93.

Nelder, J.A., Mead R, R., 1965. A simplex method for function minimization. Comput. J. 7, 308–313.

Nguyen, V.B., Wang, C.X., Thomas, C.R., Zhang, Z., 2009a. Mechanical properties of single alginate microspheres determined by microcompression and finite element modelling. Chem. Eng. Sci. 64, 821–829.

Nguyen, V.B., Wang, C.X., Thomas, C.R., Zhang, Z., 2009b. Mechanical properties of single alginate microspheres determined by microcompression and finite element modelling. Chem. Eng. Sci. 64, 821–829.

Novaretti, J.V., João, Lian, J., Patel, N.K., Chan, C.K., Cohen, M., Musah, V., Debski, R.E., 2020. Partial lateral meniscectomy affects knee stability even in anterior cruciate ligament-intact knees. J. Bone Joint Surg. 102, 567–573.

Olvera, D., Daly, A., Kelly, D.J., 2015. Mechanical testing of cartilage constructs. In: Doran, P. (Ed.), Cartilage Tissue Engineering. Humana Press, New York, pp. 279–287.

Orozco, G.A., Tanska, P., Florea, C., Grodzinsky, A.J., Korhonen, R.K., 2018. A novel mechanobiological model can predict how physiologically relevant dynamic loading causes proteoglycan loss in mechanically injured articular cartilage. Sci. Rep. 8, 1–6.

Patel, J.M., Wise, B.C., Bonnevie, E.D., Mauck, R.L., 2019. A systematic review and guide to mechanical testing for articular cartilage tissue engineering. Tissue Eng. C Methods 25, 593–608.

Quiroga, J.P., Wilson, W., Ito, K., C Van Donkelaar, C., 2017. Relative contribution of articular cartilage's constitutive components to load support depending on strain rate. Biomech. Model. Mechanobiol. 16, 151–158.

Shefelbine, S.J., Ma, C.B., Lee, K.Y., Schrumpf, M.A., Patel, P., Safran, M.R., Slavinsky, J. P., Majumdar, S., 2006. MRI analysis of in vivo meniscal and tibiofemoral kinematics in ACL-deficient and normal knees. J. Orthop. Res. 24, 1208–1217.

Walter, S.G., Ossendorff, R., Schildberg, F.A., 2019. Articular cartilage regeneration and tissue engineering models: a systematic review. Arch. Orthop. Trauma Surg. 139, 305–316.

Wilson, W., Van Donkelaar, C.C., Van Rietbergen, B., Ito, K., Huiskes, R., 2004. Stresses in the local collagen network of articular cartilage: a poroviscoelastic fibril-reinforced finite element study. J. Biomech. 37, 357–366.

Wilson, W., van Donkelaar, C.C., van Rietbergen, B., Huiskes, R., 2005a. A fibril-reinforced poroviscoelastic swelling model for articular cartilage. J. Biomech. 38, 1195–1204.

Wilson, W., Van Donkelaar, C.C., Van Rietbergen, B., Huiskes, R., 2005b. A fibril-reinforced poroviscoelastic swelling model for articular cartilage. J. Biomech. 38, 1195–1204.

Zahedmanesh, H., Stoddart, M., Lezuo, P., Forkmann, C., Wimmmer, M.A., Alini, M., Van Oosterwyck, H., 2014. Deciphering mechanical regulation of chondrogenesis in fibrin–polyurethane composite scaffolds enriched with human mesenchymal stem cells: a dual computational and experimental approach. Tissue Eng. 20, 1197–1212.